Journal of Power Sources 255 (2014) 260–265

Contents lists available at ScienceDirect

Journal of Power Sources

journal homepage: www.elsevier.com/locate/jpowsour

Electrocatalytic activity of ZnS nanoparticles in direct ethanol fuel cells

Michael Bredol [a,*], Michał Kaczmarek [a], Hans-Dieter Wiemhöfer [b]

[a] Münster University of Applied Sciences, Department of Chemical Engineering, Stegerwaldstraße 39, 48565 Steinfurt, Germany
[b] University of Münster, Institute for Inorganic and Analytical Chemistry, Corrensstraße 28/30, 48149 Münster, Germany

HIGHLIGHTS

- MEAs for direct ethanol fuel cells with ZnS/carbon-electrocatalysts were fabricated.
- Acetaldehyde and acetic acid were quantified as oxidation products.
- Mass transport and breakthrough problems caused low efficiency (maximum 25%).

ARTICLE INFO

Article history:
Received 16 July 2013
Received in revised form
27 December 2013
Accepted 29 December 2013
Available online 11 January 2014

Keywords:
Fuel cells
Electrocatalysts
Ethanol
ZnS nanoparticles

ABSTRACT

Low temperature fuel cells consuming ethanol without reformation would be a major step toward the use of renewable energy sources from biomass. However, the necessary electrodes and electrocatalysts still are far from being perfect and suffer from various poisoning and deactivation processes. This work describes investigations on systems using carbon/ZnS-based electrocatalysts for ethanol oxidation in complete membrane electrode assemblies (MEAs). MEAs were built on Nafion membranes with active masses prepared from ZnS nanoparticles and Vulcan carbon support. Under operation, acetic acid and acetaldehyde were identified and quantified as soluble oxidation products, whereas the amount of CO_2 generated could not be quantified directly. Overall conversion efficiencies of up to 25% were estimated from cells operated over prolonged time. From polarization curves, interrupt experiments and analysis of reaction products, mass transport problems (concentration polarization) and breakthrough losses were found to be the main deficiencies of the ethanol oxidation electrodes fabricated so far.

1. Introduction

The performance of direct ethanol fuel cells (DAFCs) is still limited by the electrocatalysts available for ethanol oxidation, which are mostly based on expensive noble metals such as platinum or its alloys [1–4]. From recent work, it becomes obvious, that even the facetting of single crystals of platinum nanoparticles may determine the electrochemical activity; e.g. the authors in Ref. [5] point out, that depending on the preferred orientation, either acetic acid or CO (as an intermediate to full oxidation to CO_2) are the final products of electrooxidation of ethanol on these catalysts. With CO adsorbing very strongly on platinum, the latter route leads effectively to saturation (or poisoning) of the catalyst, which hopefully will not occur when using catalysts with lesser tendency to adsorb CO.

Semiconductors, especially chalcogenides, could potentially present a solution to this problem. Initial work in this respect, investigating Zn(S,Se)-based electrocatalysts as an alternative for ethanol electrooxidation, has been published by these authors previously [6,7], explaining in detail the preparation of the catalysts and demonstrating the electrocatalytic effect of nanoparticulate ZnS in contact with ethanol, as well as the influence of the electrode composition. These early investigations were employing standard electrochemical techniques like cyclovoltammetry in a three-electrode configuration, but did not report on the performance of the working electrode in a full fuel cell setup, consuming ethanol and oxygen.

Such data however will be necessary to practically evaluate the prospects of these novel catalysts in comparison with recent progress with metal-based catalysts. Such developments are driven on one side by new metal compositions and morphologies, but also by new catalyst supports, mostly based on carbon. There are also reports about other alternatives than sulfides, e.g. with metal-organic framework materials (MOFs) based on Cu, showing electrocatalytic activity for ethanol oxidation [8]. In view of the necessary conductivity of the electrode system, it becomes more

* Corresponding author. Tel.: +49 (0)251 83 62 225.
E-mail address: bredol@fh-muenster.de (M. Bredol).

0378-7753/$ – see front matter © 2014 Elsevier B.V. All rights reserved.
http://dx.doi.org/10.1016/j.jpowsour.2013.12.142

and more obvious, that especially intimate composites of nanocarbons and inorganic semiconductors may eventually lead to alternatives for precious metals [9] on the ethanol consuming electrode. Of course, there is also need for the replacement of Pt on the oxygen electrode; from the literature it seems, that transition metal oxides might help on this side, at least this has been demonstrated in alkaline solution [10].

For this work, complete membrane electrode assemblies (MEAs) have been constructed using well-established techniques with respect to the selection of membranes, supports, gas diffusion layers etc., with the only exemption that the electrocatalyst used on the ethanol-consuming electrode has been made from carbon-supported ZnS nanoparticles; the preparation of the electrode was based on the results reported previously [6,7]. The goal was to demonstrate the usability of these novel electrocatalysts in complete fuel cells under operation, to be compared to reports on ethanol decomposition at novel metallic electrocatalysts [11,12]. The standard carbon-support chosen for this work, however, being based on traditional Vulcan carbon black, still is sub-optimal, since it is well known, that a well-ordered array of nanopores can enhance the activity still further [13,14]. There are also reports about synergistic catalytic effects inside carbon nanostructures [15], which might also be of relevance for electrocatalytic application, but are not employed yet. Further contributions to this topic can also be expected from the continuous development of new carbon structures for battery electrodes [16,17]. Meanwhile, a broad range of techniques to prepare porous carbons is available in the literature and could be used in further studies, among others by the use of soft templates [18–20], activation by burnoff [21], use of hollow spheres [22] or assemblies of graphene sheets with catalytic metal [23].

In order to be able to estimate conversion efficiencies as well as ageing behaviour from the analysis of conversion products and by-products, fuel cells constructed as MEAs from standard carbon materials with ZnS as the electrocatalyst in this work were operated under load for extended times to accumulate and analyze products.

2. Experimental

Hydrophilic ZnS-nanoparticles were prepared by arrested precipitation from zinc acetate-solution, NaHS-solution and mercaptopropionic acid (MPA) as stabilizing ligand, as described in Refs. [6,7].

MEAs with ZnS as oxidation catalyst were fabricated according to the slightly modified state-of-the-art technique as described in the literature e.g. by Tang et al. [24] and by Lindermeir et al. [25]. Briefly, gas diffusion layers (GDLs) were prepared by deposition of a slurry of isopropanol, carbon and Teflon on a teflonated (30%) carbon paper (substrate and electron collector) by tape casting (so-called "doctor-blading": the slurry is deposited on the substrate through the opening in a flat steel mask of ca. 50 μm thickness, using a sharp knife to define the amount of material transferred through the mask). Isopropanol was mixed with Vulcan XC-72 and Teflon dispersion and ultrasonicated for 30 min. The resulting slurry was then further homogenized with a high speed homogenizer for 30 min.

The highly-viscous paste was tape cast on carbon paper pieces (9 cm^2) to reach a carbon load of 8 mg cm^{-2} (measured as dry mass of carbon). The resulting GDL was then sintered in an oven at 335 °C for 120 min in air.

The fuel electrode was prepared by mixing deionized water with 5 wt% Nafion dispersion and carbon-supported ZnS:Mn nanocrystals (the mixture of carbon and the nanoparticles was prepared before from water dispersion of the nanoparticles and dried in an oven for 12 h at 40 °C, under vacuum). The mixture was first ultrasonicated for 30 min and then homogenized to achieve a printable paste.

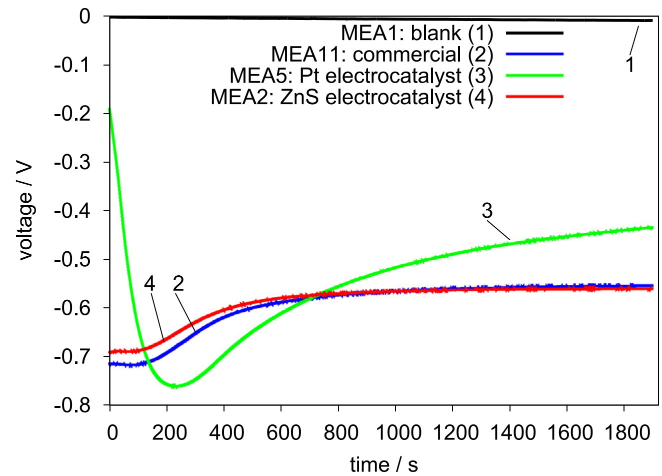

Fig. 1. Open circuit voltage (V_{oc}) as a function of operation time. MEA1: blank, carbon electrode only. MEA2: with ZnS electrocatalyst in fuel electrode. MEA5: with Pt electrocatalyst in fuel electrode. MEA11: commercial Pt-based MEA.

The paste was applied by tape casting onto the GDL to reach catalyst loads from 3 mg cm^{-2} to 12 mg cm^{-2} (calculated from the dry mass). The electrode was finally dried for 30 min at 90 °C. Fabrication of the oxygen electrode was similar to the fabrication process of the fuel electrode; ZnS catalysts however were replaced by carbon-supported platinum (20 wt%), supplied by *Fuel Cell Earth*. The catalyst slurry prepared was tape-casted on the GDL to achieve a catalyst load of 2 mg cm^{-2}.

The last stage was hot pressing of all components (pre-treated nafion membrane, anode and cathode) at 140 °C with 10 MPa. In order to ensure good adhesion between the Nafion membrane and both electrodes, anode and cathode were sprayed with a small amount of 5 wt% Nafion dispersion just before the pressing step. After hot pressing, the freshly prepared MEAs, with an active area diameter of 9 cm^2, were dried in air and stored for measurements under ambient conditions. For comparison, MEAs prepared with Pt instead of ZnS in the fuel electrode were prepared in a similar fashion. Commercial MEAs were purchased for comparison from the *Fuel Cell Store*.

All cells were operated with ethanol/water mixtures (typically 3% ethanol by weight) as fuel and air as oxygen source. In order to establish steady state conditions, the cells were mounted in contact with a sufficiently large amount of fuel housed in an acrylic glass container. Air was supplied by natural convection at ambient pressure (passive breathing mode). Operation usually took place at ambient (room) temperature; for operation at increased temperature the fuel container was placed in a thermostate.

Electrochemical data and impedance spectra of complete cells have been recorded using a *Zahner IM6 Electrochemical Workstation*, acquiring data with the *Thales* acquisition software; a simple two-electrode-configuration was used for all measurements. Apart from DC potentiostatic (e.g. I_{sc}, $V = 0$) and galvanostatic (e.g. V_{oc}, $I = 0$) modes of operation, AC measurements were performed at frequencies from 100 mHz to 1 MHz. The electrochemical impedance spectra data (EIS) were fit to the appropriate model of an electrical equivalent circuit (EEC) using the *ZSimpWin 3.10* software (*Princeton Applied Research*, U.S.A.), utilizing the complex non-linear least square error technique (CNLS).

The qualitative and quantitative analysis of reaction products has been conducted at a *Shimadzu* gas chromatograph equipped

with a *Shimadzu* QP2010 mass spectrometer. The separation column applied was filled with polystyrol-divinylbenzol copolymer (PS-DVB). For analysis, 0.3 μl of freshly prepared sample has been collected from the reaction mixture at predefined times. The method has been calibrated with acetaldehyde or acetic acid added to solutions with 3% of ethanol.

3. Results and discussion

The cells prepared according to the procedure explained in the experimental (using air as the O_2-source) reached open circuit voltage values (V_{oc}) of about 0.6 V after prolonged operation, which is ca. 50% of the theoretically maximal value (1.14 V) and is on the same order as reported for MEAs with Pt/Ru-catalysts [11]. This level is kept after an initial decrease of V_{oc}, probably due to formation reactions in the electrode. Fig. 1 compares this behaviour with blanks and bench marks, namely MEAs prepared without electrocatalyst (negligible voltage), with Pt instead of ZnS, and a commercially available MEA. The ZnS-loaded MEAs are showing characteristics close to the commercial variant, and much more favourable behaviour than the home-made variant with Pt nanoparticles. Obviously, there are still considerable overvoltages for all MEA variants shown in Fig. 1 and thus there is much room for further improvements.

Observing short-circuit current densities (I_{sc}) leads to a slightly different picture. Due to the far better electrical conductivity, the home-made MEA with Pt (albeit at quite high catalyst load) shows the highest value for I_{sc}, but also a constant decline over operation time (Fig. 2).

The cell characteristics will depend crucially on the microstructure of the electrodes. Fig. 3 shows electron micrographs of the carbon/ZnS composite, demonstrating that the overall distribution of the catalytic particles (upper micrograph) is non-uniform, and that only a fraction of the individual particles are coupled to the conductive carbon support (bottom left). The individual ZnS particles on the other hand have primary particle sizes of about 10–20 nm in diameter (bottom right) – these images clearly show the potential for further morphological improvement of the electrode materials. Since the purpose of this work was to investigate ZnS-based electrocatalysts under operation in an MEA, Pt-based catalysts were prepared and compared as a bench mark only to demonstrate, that the general procedure of MEA fabrication was successful. Since the microstructure of the ZnS/carbon electrode still offers much room for improvement and is far from being optimal, investigations on home made Pt-catalysts were discontinued; further results with ZnS/carbon electrodes thus were compared to commercially available Pt-based catalysts only.

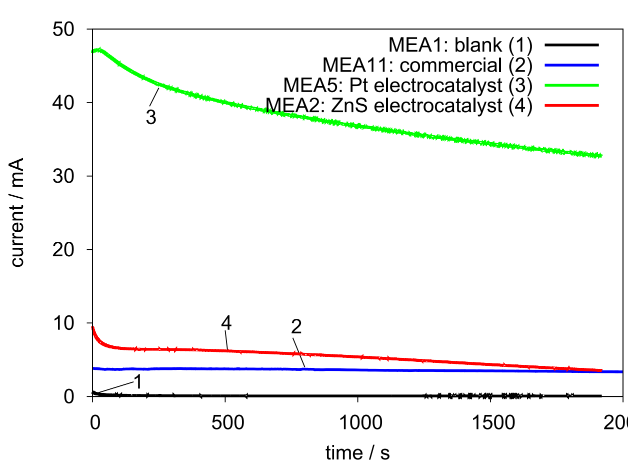

Fig. 2. Short circuit current (I_{sc}) as a function of operation time. MEA1: blank, carbon electrode only. MEA2: with ZnS electrocatalyst in fuel electrode. MEA5: with Pt electrocatalyst in fuel electrode. MEA11: commercial MEA.

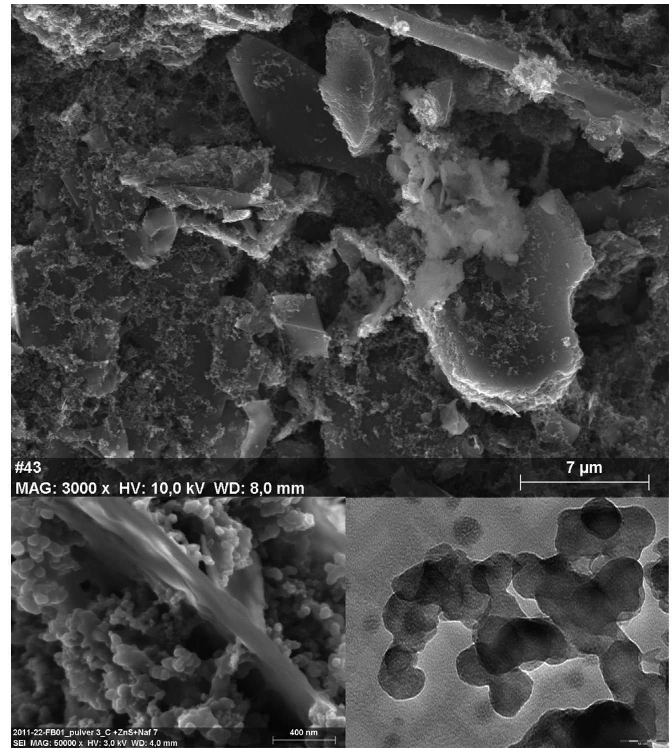

Fig. 3. Electron micrographs of carbon (large particles)/ZnS (small particles) composite mass for electrodes. Top: SEM-image of lateral distribution (scale bar: 7 μm). Bottom left: SEM-image of individual C-particle with ZnS nanoparticles (scale bar 400 nm). Bottom right: TEM-image of individual ZnS particles (scale bar 50 nm).

MEA2 (containing the ZnS electrocatalyst) and the commercial alternative on the other hand also show some ageing with operation time, with MEA2 exhibiting a short formation period, followed by more constant operation conditions. Improved conductivity of the electrodes and a more even dispersion of the ZnS electrocatalyst would be the most obvious strategies to further improve these characteristics.

An application oriented way to characterize fuel cells and batteries under load is the polarization curve, which plots cell voltage (or extracted power) versus the current drawn; Fig. 4 displays this behaviour for the same MEAs as in Figs. 1 and 2, but without MEA5 with its unusually high catalyst load.

All polarization curves exhibit strongly negative slopes and consist of two parts, which can be distinguished clearly by their different slopes, quite similar to those reported e.g. in Ref. [11]. This appearance indicates problems with mass transport in the electrode or insufficient electrocatalytic activity. Obviously, the particles are still neither perfectly dispersed nor homogenously distributed. Moreover, bigger agglomerates could limit the catalytic activity since their individual particles then are only partially attached to the carbon surface. Such agglomerates can also lead to poor mass transport in the electrode through prolonged diffusion paths. Further work will be necessary to improve on the obviously sub-optimal preparation conditions.

Using the current interrupt technique, the relative importance of ohmic and activation losses can be determined; Fig. 5 shows the result of such measurements. In the first step of the measurement the galvanostat was set to 50 μA for about 40 min. One can see that the potential during this time decreases in the beginning, to

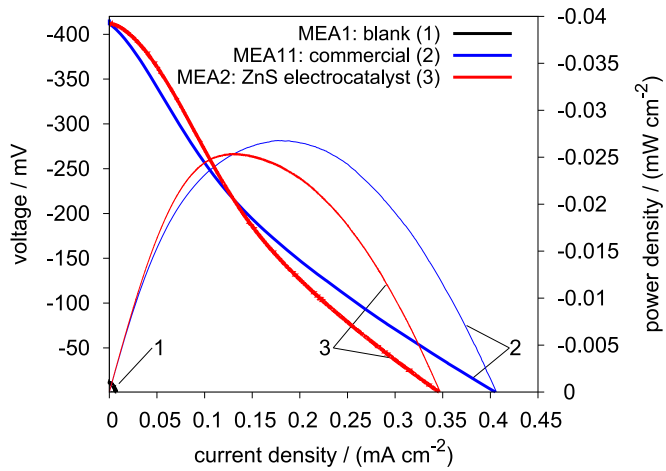

Fig. 4. Polarization curve (thick line) and power density (thin line) as a function of current. MEA1: blank, carbon electrode only. MEA2: with ZnS electrocatalyst in fuel electrode. MEA11: commercial MEA.

become almost stable after about 25 min. At that moment the current has been stopped (galvanostat set to 0 μA), resulting in voltage recovery. A fast initial change of the recorded voltage is a consequence of the immediate reduction of ohmic losses to 0; this is found to a minor extent in MEA11, but is barely visible in the ZnS-containing MEA2. Obviously, relaxation of concentration polarization effects is the dominating mechanism, especially with the ZnS catalysts. This is in good agreement with the conclusions drawn before, namely that the expected mass transport problems in the environment of ZnS could be minimized by a better dispersion and more homogenous distribution of catalytic nanoparticles at the surface of the carbon substrate; this would also help to reduce remaining ohmic losses.

$$V(t) = V_{eq} + (V_{eq} - V_{load})e^{-k(t-t_0)} \quad (1)$$

Relaxation based on transport may occur over many time scales and also with higher order kinetics. Attempts to fit the curves in Fig. 5 to a single exponential function with one characteristic time constant k (Equation (1)) between the equilibrium voltage V_{eq} and the voltage under load before interrupt at time $t = t_0$ (V_{load}) therefore were not successful; see the inset of Fig. 5 with $k = 0.011$ s^{-1} as an example for the earlier stages of relaxation. Characteristic relaxation times therefore cannot be extracted unambiguously at this point, but obviously range between seconds and many minutes. A similar behaviour (although on shorter time scales) was analyzed in the case of solid oxide fuel cells (SOFC) to extract a "distribution of relaxation times" from EIS, indicative of the polarization mechanisms involved [26].

Activation losses in general however seemed to be very similar for all electrodes investigated, what means that the main problem to be solved in future work, is the still poor distribution of ZnS nanocrystals on the electrode surface, causing mass transport problems.

In order to assess the types of existing overvoltages in more detail, electrochemical impedance spectra of various electrodes have been recorded and compared (for an example, see Fig. 6 with data collected with MEA2 at two different operation temperatures under load, with cell voltage −0.1 V and an AC amplitude of 5 mV). The interpretation takes place by an equivalent circuit containing RC-circuits for the membrane as well as for the working electrode (Fig. 7; the inductivity originally proposed in Ref. [27] has been omitted in view of the small currents used here). The circuit for the electrode contains a double layer capacity as well as a constant phase element (CPE, $Z = (1/Q)(i\omega)^{-\alpha}$) in order to be able to include transport phenomena in a flexible way. The χ^2 (chi-squared) values obtained for all successful fits were at least as small as 10^{-4}; other results or fit results with non-physically large values for the capacities were rejected, since they are dominated most probably by artefacts not related to the working electrode and its electrocatalytic activity.

In Table 1, the parameters of fitting the measured data of Fig. 6 to the EEC of Fig. 7 are listed. Not surprisingly, all resistances shrink when increasing the temperature. At both temperatures the membrane resistance is larger than the charge transfer resistance; together with the serial (electrolyte) resistance this does account for the majority of the ohmic losses.

Moreover, an approximately straight line with slope of ca. 45° can be observed in all spectra at low frequencies; this is related to mass transport limitations of the fuel electrode. The constant phase element (CPE) in Fig. 7 as proposed in Ref. [27] shows values for the exponent α close to 0.5 and thus could be replaced also by a simple *Warburg*-element. Further elements for details of the reaction

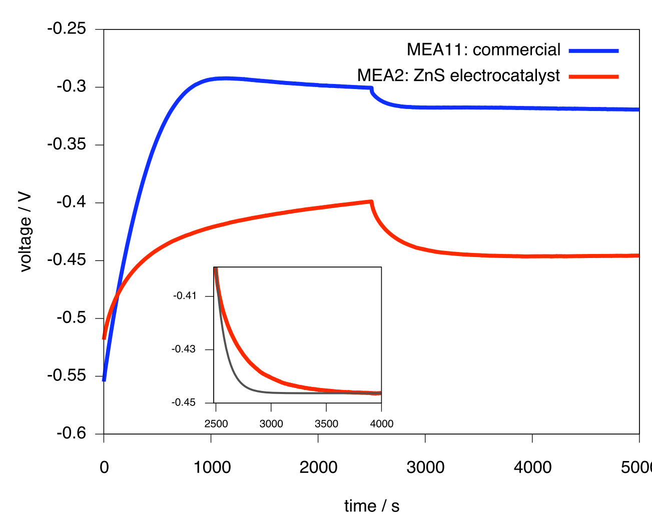

Fig. 5. Cell voltage curve versus time in current interrupt experiments. MEA2 (lower line): with ZnS electrocatalyst in fuel electrode. MEA11 (upper line): commercial MEA. Inset: relaxation part of MEA2 (thick line), compared to single exponential relaxation with $k = 0.011$ s^{-1} (grey, thin line).

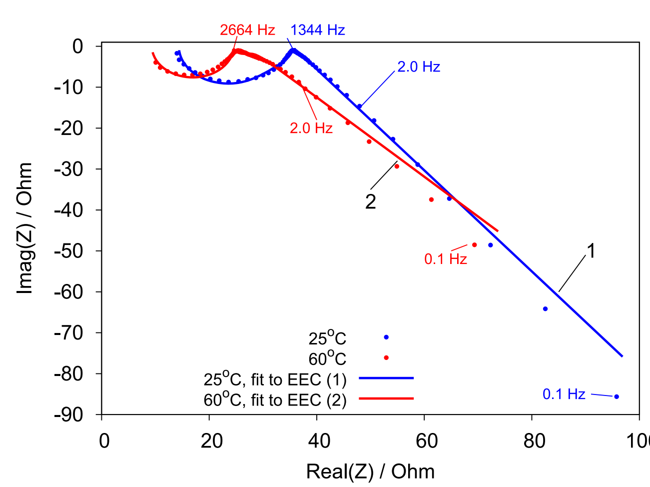

Fig. 6. Impedance spectra of MEA2 at various temperatures (points), together with fits to the EEC according to Fig. 7 (lines). Frequency is used as parameter and indicated at typical values, cell voltage −0.1 V, AC amplitude 5 mV.

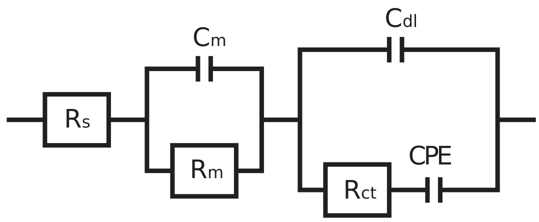

Fig. 7. Equivalent circuit for the interpretation of impedance spectra according to [27]; R_S: serial ohmic resistance, C_m: membrane capacity, R_m: membrane resistance, C_{dl}: double layer capacity, R_{ct}: charge transfer resistance, CPE: constant phase element.

kinetics have not been added at this stage of interpretation, since it seems obvious, that mass transport problems have to be solved first in future studies. Such studies could focus on the electrocatalytical activity of other sulfides, e.g. pyrite with its high photocatalytic activity [28], or try to improve the morphology of the electrocatalytic system, e.g. by the application of electrocatalytic layers with controlled porosity on conducting substrates. Preparational methods for ZnS in this context are already available from the literature [29], as well as for other porous sulfides, since they are also of interest for lithium storage in batteries [30].

With GC–MS analysis, all reaction products but CO_2 could be separated clearly from the fuel (ethanol); with increasing reaction time the amount of ethanol (the highest peak at about 2.8 min) decreases proportionally, and peaks of acetaldehyde (around 2.7 min retention time) and acetic acid (4.3 min retention time) are formed (Fig. 8). This result demonstrates unambiguously, that MEAs with ZnS electrocatalysts convert ethanol directly in a fuel cell setup. Whereas acetaldehyde was formed immediately, acetic acid could be detected after 4 h only; acetaldehyde therefore seems to be formed as a stable intermediate immediately. The increase of the amounts of acetaldehyde and acetic acid with time can be observed as well. However, after prolonged operation time under short circuit conditions, the concentration of acetaldehyde tends to reach a plateau (which is typical for an intermediate product), whereas the concentration of acetic acid tends to increase still, proportional to operation time. In fact, after 27 h the concentration of acetic acid is roughly 5 times larger than the concentration of acetaldehyde, clearly demonstrating the ability of the ZnS electrocatalyst to support the multistep processes necessary for ethanol consumption. Future work with improved cell designs will have to establish these relations more quantitatively, especially in view of the amount of CO_2 generated, and whether acetic acid will reach a concentration plateau as well. Ethyl acetate is observed as an additional reaction product; the origin of this compound can be explained as a result of recombination of acetic acid with ethanol at the ZnS catalyst or during sample evaporation before supplying it to the detection column.

In order to separate product formation by electrocatalytic conversion from product formation by breakthrough processes (direct oxidation of ethanol by O_2 after penetration of the membrane), analytical data from cells operated under short-circuit-condition and under open-circuit-condition are compared in Fig. 9.

Whereas acetaldehyde is present on a quasi-stationary level also under open-circuit-conditions, acetic acid is increasing its concentration continuously, in line with the view, that acetaldehyde

Table 1
Results of fitting data from Fig. 6 to the EEC of Fig. 7.

	R_s/Ω	R_m/Ω	C_m/nF	R_{ct}/Ω	C_{dl}/μF	α	$Q/(\Omega^{-1}\ s^{\alpha})$
25 °C	14.36	17.01	54.2	4.095	1.597	0.5667	0.01333
60 °C	9.35	15.15	34.4	2.913	50.850	0.4914	0.01938

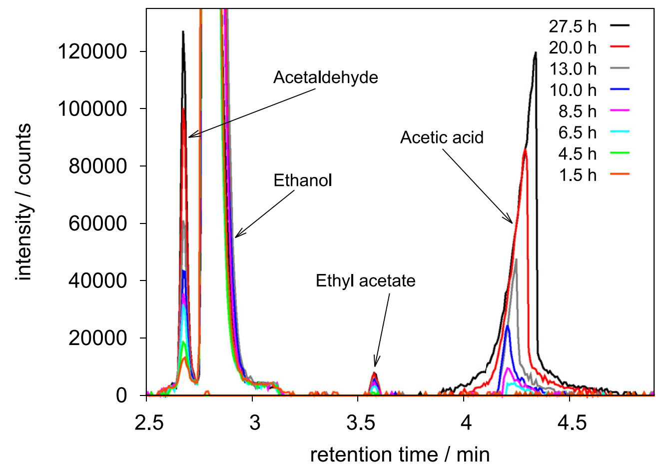

Fig. 8. GC–MS analysis of oxidation products after operation of MEA 2 for several hours; traces are stacked exactly in order of operation time.

always is formed as an intermediate during oxidation of ethanol. Under full electrical load (short circuit), the level of acetaldehyde as well as the level of acetic acid are increasing over time by approximately an order of magnitude, clearly demonstrating, that electrocatalytic conversion becomes the dominant process.

In order to compare electrochemical conversion and breakthrough processes more quantitatively, after 27.5 h of operation the absolute molar amounts of acetic acid (3.37 mmol) and acetaldehyde (1.06 mmol) generated were used to calculate the maximum charge that could be provided by oxidation of ethanol to these end products: ca. 1500 As. From the integrated current/time curve, a transferred charge of ca. 650 As was observed. Assuming that no CO_2 was generated, approximately 50% of the fuel therefore was lost in breakthrough processes, possibly even more, when CO_2 was generated, too. Together with losses from overvoltages (open circuit voltage is about half of the thermodynamic equilibrium value), the MEAs tested thus showed an overall efficiency (electrical work relative to free fuel energy) of less than 25%.

4. Conclusions

In this work, MEAs for direct ethanol fuel cells with nano-ZnS as electrocatalyst have been fabricated and tested for the first time.

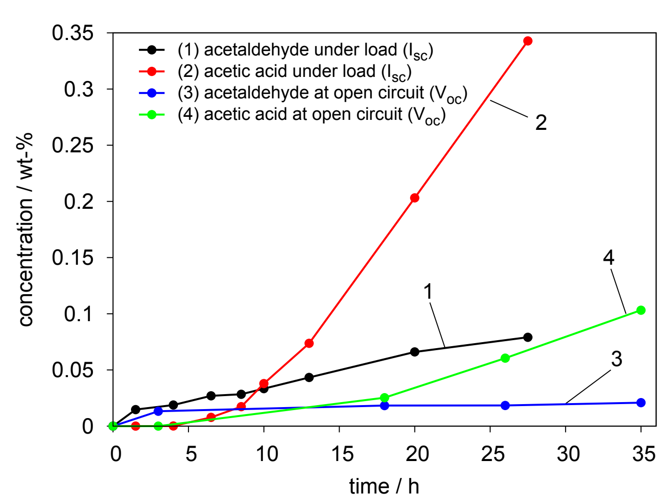

Fig. 9. GC–MS analysis of oxidation products after operation of MEA 2 under short-circuit-condition and under open-circuit-condition.

From the analysis of electrical cell data, the polarization curves under load and the chemical analysis of the electrolyte, the electrocatalytic activity has been demonstrated clearly under the conditions of a full fuel cell setup. Limitations in performance under load so far are dominated mainly by mass transport problems (concentration polarization) and to a minor extent by conductivity issues of the carbon/ZnS nanocomposite. Overvoltages are considerable (ca. 50% of the equilibrium value). Imperfections of the cell construction have led to breakthrough processes in the full assembly. A remaining principal problem as compared to electrocatalysts based on noble metals is the chemical turnover to CO_2 achievable with ZnS electrocatalysts; any practical application will depend critically on the efficiency by which the fuel can be exploited. Future work therefore will have to address the issue of conversion efficiency of ethanol to CO_2 first; of course on top of this issue electrode morphology, general catalyst activity and cell construction will have to be improved as well to be able to fully exploit ZnS or other sulfides as potential electrocatalysts. Still more work will be necessary to identify the detailed catalytic mechanism of the ZnS-containing electrodes.

Acknowledgements

Parts of this work were supported by the European Union and the Federal State of North-Rhine-Westphalia in Germany in the framework of an EFRE project (European Fund for Regional Development).

References

[1] K.-Y. Chan, J. Ding, J. Ren, S. Cheng, K.Y. Tsang, J. Mater. Chem. 14 (2004) 505–516.
[2] H. Wang, Z. Jusys, R.J. Behm, J. Phys. Chem. B 108 (2004) 19413–19424.
[3] F. Vigier, S. Rousseau, C. Coutanceau, J.-M. Leger, C. Lamy, Top. Catal. 40 (2006) 111–121.
[4] G. Siné, D. Smida, M. Limat, G. Fóti, C. Comninellis, J. Electrochem. Soc. 154 (2007) B170–B174.
[5] C. Busó-Rogero, V. Grozovski, F.J. Vidal-Iglesias, J. Solla-Gullón, E. Herrero, J.M. Feliu, J. Mater. Chem. A 1 (2013) 7068–7076.
[6] M. Bredol, M. Kaczmarek, J. Phys. Chem. A 114 (2010) 3950–3955.
[7] M. Kaczmarek, M. Bredol, J. Mater. Sci. 46 (2011) 5400–5405.
[8] L. Yang, S. Kinoshita, T. Yamada, S. Kanda, H. Kitagawa, M. Tokunaga, T. Ishimoto, T. Ogura, R. Nagumo, A. Miyamoto, M. Koyama, Angew. Chem. Int. Ed. 122 (2010) 5476–5479.
[9] Y. Liang, Y. Li, H. Wang, H. Dai, J. Am. Chem. Soc. 135 (2013) 2013–2036.
[10] H. Zhu, S. Zhang, Y.-X. Huang, L. Wu, S. Sun, Nano Lett. 13 (2013) 2947–2951.
[11] J. Mann, N. Yao, A.B. Bocarsly, Langmuir 22 (2006) 10432–10436.
[12] A. Kowal, M. Li, M. Shao, K. Sasaki, M. Vukmirovic, J. Zhang, N. Marinkovic, P. Liu, A. Frenkel, R. Adzic, Nat. Mater. 8 (2009) 325.
[13] J. Zhao, F. Cheng, C. Yi, J. Liang, Z. Tao, J. Chen, J. Mater. Chem. 19 (2009) 4108–4116.
[14] C. He, Y. Liang, R. Fu, D. Wu, S. Song, R. Cai, J. Mater. Chem. 21 (2011) 16357–16364.
[15] X. Pan, Z. Fan, W. Chen, Y. Ding, H. Luo, X. Bao, Nat. Mater. 6 (2007) 507–511.
[16] D.-Y. Kang, S.-O. Kim, Y.J. Chae, J.K. Lee, J.H. Moon, Langmuir 29 (2013) 1192–1198.
[17] X. Ji, K.T. Lee, L.F. Nazar, Nat. Mater. 8 (2009) 500–506.
[18] X. Yan, H. Song, X. Chen, J. Mater. Chem. 19 (2009) 4491–4494.
[19] H.-J. Liu, W.-J. Cui, L.-H. Jin, C.-X. Wang, Y.-Y. Xia, J. Mater. Chem. 19 (2009) 3661–3667.
[20] L. Chuenchom, R. Kraehnert, B.M. Smarsly, Soft Matter 8 (2012) 10801–10812.
[21] D. Wu, Y. Liang, X. Yang, C. Zou, Z. Li, G. Lv, X. Zeng, R. Fu, Langmuir 24 (2008) 2967–2969.
[22] C. Galeano, J.C. Meier, V. Peinecke, H. Bongard, I. Katsounaros, A.A. Topalov, A. Lu, K.J.J. Mayrhofer, F. Schüth, J. Am. Chem. Soc. 134 (2012) 20457–20465.
[23] L. Ren, K.S. Hui, K. Hui, J. Mater. Chem. A 1 (2013) 5689–5694.
[24] H. Tang, S. Wang, S.P. Jiang, M. Pan, J. Power Sources 170 (2007) 140–144.
[25] A. Lindermeir, G. Rosenthal, U. Kunz, U. Hoffmann, J. Power Sources 129 (2004) 180–187.
[26] H. Schichlein, A. Müller, M. Voigts, A. Krügel, E. Ivers-Tiffée, J. Appl. Electrochem. 32 (2002) 875–882.
[27] R.E. Melnick, G.T.R. Palmore, J. Phys. Chem. B 105 (2001) 1012–1025.
[28] A. Kirkeminde, S. Ren, J. Mater. Chem. A 1 (2013) 49–54.
[29] A. Fischereder, M.L. Martinez-Ricci, A. Wolosiuk, W. Haas, F. Hofer, G. Trimmel, G.J.A.A. Soler-Illia, Chem. Mater. 24 (2012) 1837–1845.
[30] X. Yin, C. Tang, M. Chen, S. Adams, H. Wang, H. Gong, J. Mater. Chem. A 1 (2013) 7927–7932.